Independence of Slip Velocities on Applied Stress in Small Crystals

R. Maaß, P. M. Derlet, and J. R. Greer*

Directly tracing the spatiotemporal dynamics of intermittent plasticity at the micro- and nanoscale reveals that the obtained slip dynamics are independent of applied stress over a range of up to ~400 MPa, as well as being independent of plastic strain. Whilst this insensitivity to applied stress is unexpected for dislocation plasticity, the stress integrated statistical properties of both the slip size magnitude and the slip velocity follow known theoretical predictions for dislocation plasticity. Based on these findings, a link between the crystallographic slip velocities and an underlying dislocation avalanche velocity is proposed. Supporting dislocation dynamics simulations exhibit a similar regime during microplastic flow, where the mean dislocation velocity is insensitive to the applied stress. Combining both experimental and modeling observations, the results are discussed in a framework that firmly places the plasticity of nano- and micropillars in the microplastic regime of bulk crystals.

1. Introduction

The onset of local plastic flow in bulk metals is known to be notoriously difficult to access in both space and time, but it determines the strength of a turbine blade in your aircraft or an axel shaft in your car. Structural changes, such as a collective defect reorganization in a crystal—otherwise known as a dislocation avalanche—are remarkably fast as well as spatially confined to the micro- or nanometer length scale. Historically, driven by the desire to better understand plastic flow, great efforts have been undertaken to investigate the movement of both individual dislocations[1–5] and groups of dislocation groups.[6–13] The used techniques have been applied at different temperatures, for different crystals, for different dislocation densities and under various stress conditions, all showing that dislocation motion in metals, at temperatures below ca. half the melting point, is a thermally activated mechanism that is highly stress-dependent.[14] In soft fcc metals, dislocations reach their highest speeds due to the low Peierls-barrier. The strong velocity-stress scaling is found for both individual as well as groups of dislocations, but with widely scattered data and with some inconsistent trends. For instance, single dislocations have been shown to move at speeds of ~10 ms^{-1} in pure Cu,[15] but dislocation groups moved with ~10^{-6} ms^{-1} in Cu-0.5%Al.[16] The opposite is found for Fe, where dislocation groups are found to move six orders of magnitude faster in a FeSi-alloy than individual dislocations in pure iron.[6,17] In Zn the scatter among dislocation-group velocities ranges between ~1 to 10^2 ms^{-1}, demonstrating the sensitivity of the results to the fine details of the microstructure as well as on the measurement technique. Despite the large variations in velocity, a consistent picture emerges with respect to the different velocity-stress scaling regimes. At very high velocities of ~1–$10^2 ms^{-1}$ an approximately linear regime dominated by viscous drag is found, whereas a power-law relation or an exponential scaling describes well the much stronger stress-dependent motion at lower dislocation velocities. The most widely used method to establish the above findings is the investigation of etch pits before and after an application of a defined stress pulse, as also used in the original work by Johnston and Gilman.[1] Other techniques relying on electron microscopy,

Dr. R. Maaß, Prof. Dr. J. R. Greer
Division of Engineering and Applied Science
California Institute of Technology
Pasadena, CA 91125–8100, USA
E-mail: robert.maass@ingenieur.de

Dr. P. M. Derlet
Paul Scherrer Institut
Condensed Matter Theory
CH-5232, Villigen, Switzerland

DOI: 10.1002/smll.201400849

X-ray topography or slip line analysis have been used as well, all of which have their specific advantages and limitations. A detailed description of these techniques can be found in the literature.[14,18]

Whilst the majority of dislocation velocity measurements use different imaging techniques combined with either mechanical data or time resolved topological data, recent developments in small scale mechanical testing now allow to directly correlate the intermittency of collective dislocation motion with the mechanical response by studying discrete events in stress and strain. Testing micro- or nano-scale metallic objects reveals a rich and detailed stochastic flow signature, where advantage is taken of sub-nanometer resolution in displacement and sub-micro-Newton resolution in force. In such tests, discrete forward surges in displacement are frequently measured, which have been shown to directly correspond to dislocation avalanches[19–21] triggered by the constantly evolving dislocation structure. Currently, the most prominent method in this context is a miniaturized compression experiment, where a nanoindenter equipped with a flat indentation tip is used.[22,23] This either micro- or nano-compression experiment has subsequently been developed further to in-situ techniques in combination with transmission electron microscopy (TEM),[24] scanning electron microscopy (SEM),[25,26] and micro-diffraction methods.[27–29] Besides reinvigorating interest in intermittent plastic flow, small scale mechanical testing has revealed intriguing extrinsic size-scaling effects.[30–33]

In this work, we use the high displacement resolution of a displacement controlled micro-compression experiment, combined with kHz data acquisition rates (DAR) to study the spatio-temporal properties of intermittent collective dislocation activity in the form of displacement jumps. Such data gives quantitative insight into slip velocities which are subsequently discussed in terms of groups of moving dislocations and thus dislocation avalanches. When testing Au single micro- and nanocrystals covering a sample size range between 300 nm and 5 μm, our results show that the slip velocity does not scale with the externally applied stress. Independent of crystal size, and therefore stress, we find a resolved mean slip velocity of ~10^{-5} ms^{-1}, where additionally no influence of plastic strain can be found. We combine our experimental results with two dimensional dislocation dynamics simulations (2D DD), and find a similar regime of behavior, where a scaling between the applied stress and dislocation velocity is absent. This independence of applied stress seen in both experiment and simulation is rationalized by the dominance of internal stress fluctuations which exceed the applied stress during the occurring instability of a dislocation avalanche. Such an interpretation leads naturally to the assertion that plastic flow in metallic micro- and nano-pillars proceeds equivalently to the micro-plastic regime of a bulk specimen.

2. Results

2.1. Intermittent Size-Dependent Plastic Flow

The stress-strain data presented in **Figure 1** shows intermittent plastic flow for sample sizes between 300 nm and 5 μm, and is very similar to earlier studies on size-affected crystal plasticity.[30–34] A 2 μm sample before and after compression is shown in Figures 1b and c respectively. Deriving the flow stresses at either 5 or 10% strain yields stress-values for the individual samples that follow the typical stress-size scaling trend of $\sigma_{\text{flow}} \propto D^{-0.6}$, with D being the diameter and σ_{flow} the flow stress. An inset in Figure 1 shows a zoom-in on a single strain burst, which is a signature of a crystallographic slip event and thus a dislocation avalanche. Each slip event is followed by a stress drop. The stress drop is a result of the feedback loop that controls the displacement rate. The feedback control recognizes, during or after an event, that the current displacement is too far relative to the programmed value at that time. As a result, the device retracts the compression tip to the position where it ought to be at that moment, resulting in a linear elastic unload and reload that is characteristic for flow curves obtained with displacement controlled testing.

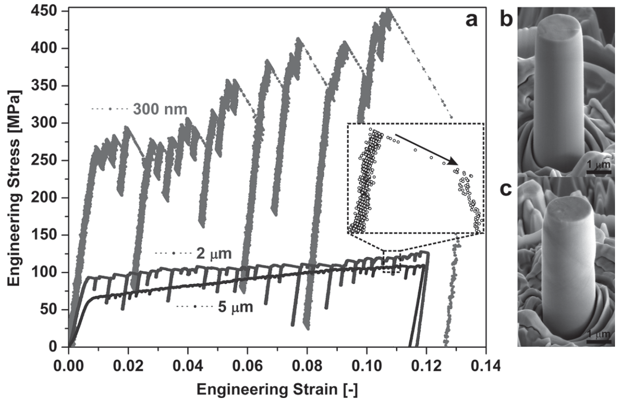

Figure 1. a) Engineering stress-strain data of cylindrical Au ⟨001⟩-oriented single crystals for three different sample sizes. The inset highlights a strain jump that is a signature of a dislocation avalanche. Panels (b) and (c) show a 2 μm sample before and after compression, respectively.

We note at this stage, that there is an apparent increase in the strain-jump magnitude with decreasing sample size, which will be treated in terms of absolute displacement magnitude in the following sections. All samples have been strained to approximately 12%, and the number of events per sample increases for larger samples. As will be shown, this is due to similar displacement jump magnitudes for all sample sizes studied. Thus, a higher number of small samples had to be tested, in order to analyze a statistically comparable set of events per sample size.

2.2. Analysis of Slip Velocities

All compression experiments were done with intentionally avoiding data binning, which in combination with the high DAR increases the noise amplitude of the acquired data to well above the specified noise-floor values of 0.2 nm and 0.06 μN, respectively. By measuring the displacement at a contact force of 1 μN prior to the deformation test, we determine the difference between the maximum and minimum displacement value to be ~0.8 nm. This value represents a conservative threshold value for the detection of a displacement jump. Since it is possible that the difference between

DOI: 10.1002/smll.201400849

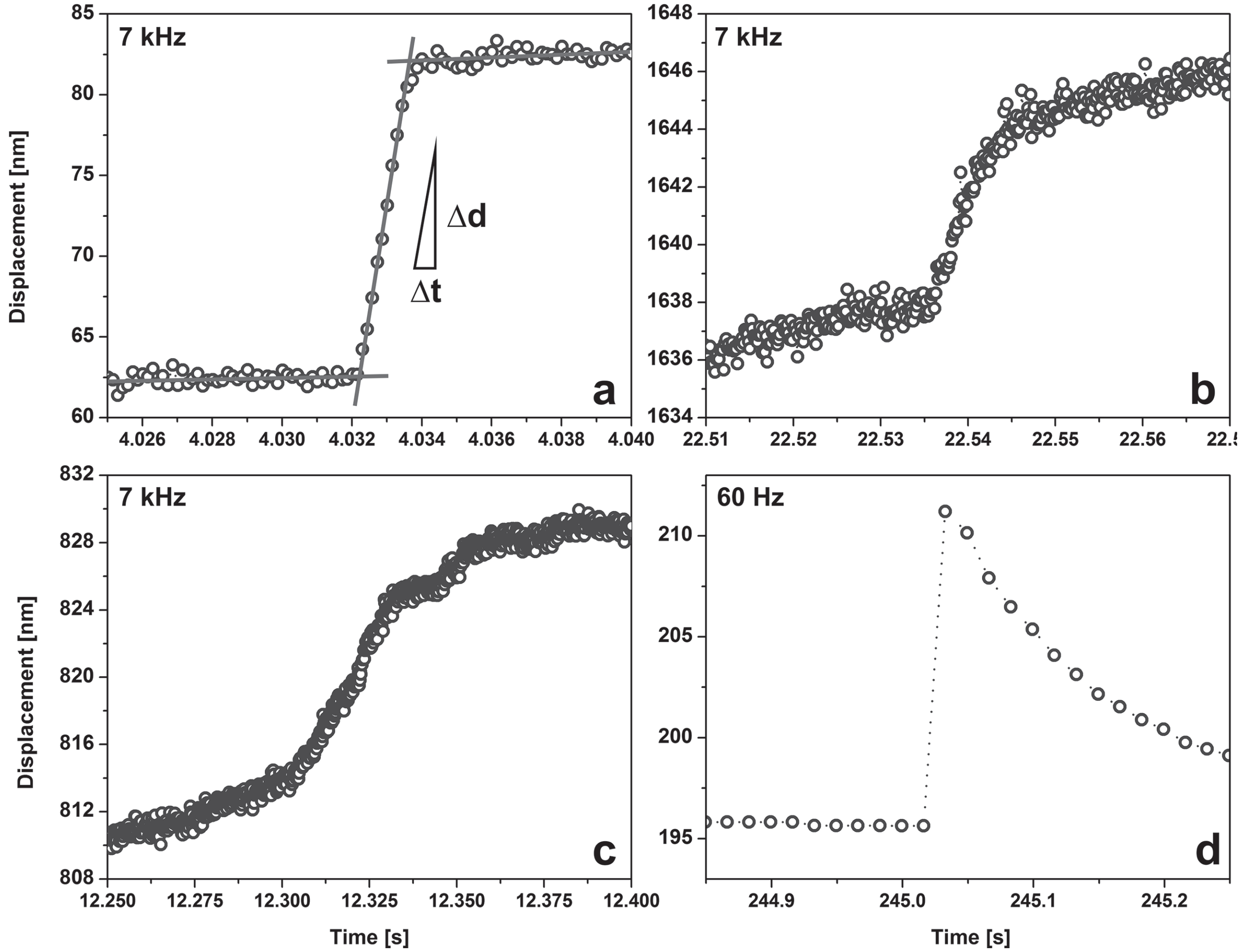

Figure 2. Four different types of displacement jumps which can be observed: a) a quick linear increase in displacement vs. time that is termed a "fast" event; b) a "slow" displacement jump which is oversampled by the DAR; c) a displacement jump with a complex substructure which does not allow for a meaningful determination of the mean slip velocity, and; d) a displacement jump obtained with a low DAR rate that does not allow a correct determination of an equivalent slip velocity. In (d), the reduction in displacement after the event (also occurring in (a–c), but not shown due to the short time window in the figures) is due to the system returning to its predefined displacement-time relation.

a series of a few data points exceed the threshold value of 0.8 nm, but afterwards the data points drop down to the same noise level as before, a local jump in displacement exceeding the threshold was not sufficient for a detection. In addition, it was also required that the mean of the data just prior to and after the event was different by this threshold. A semi-automated Matlab routine was used to analyze the detected displacement jumps, followed by a manual inspection of each event.

Looking closely at the slip events (displacement jumps) for all samples, shows that the events can be categorized into three different classes. Most events evidence a clear monotonous increase in displacement as a function of time, where data points line up in a linear fashion (**Figure 2**a). This kind of slip event, which we will term as "fast", offers an unambiguous determination of both its magnitude Δd and its duration Δt, by fitting a linear model to the data before, during and after the displacement jump, as is shown in Figure 2a. The intersection points of the linear fits will be taken as the beginning and end points of the events allowing for the calculation of a resolved average slip velocity. A second category termed, "slow", also exhibits a linear rise in displacement as a function of time, but has a higher data point density along the displacement increase (Figure 2b). In this case the high DAR over samples the event and it cannot be known whether the event represents a single jump within the limits of the experimental means, or if there are multiple small consecutive events occurring. In such a case, we also derive a mean slip velocity, which represents the entire jump in displacement. Thirdly, there are "slow" cases where the displacement jump is clearly detectable in its overall magnitude, but from the signal a complex substructure is observed at a scale that renders an average determination of any displacement-jump size or duration as being meaningless (Figure 2c). Such complex events are rare (for example 3% of all events of the 2 μm specimens). Thus, in the following we will distinguish between regular but "fast" (Figure 2a), and "slow" (Figure 2b) slip velocities. It is acknowledged that this categorization may appear ad-hoc, but we will later show that this separation can indeed be motivated by the different trends observed.

Whilst the used DAR of 7 kHz increases the noise of the measured data, it is required to sample an occurring

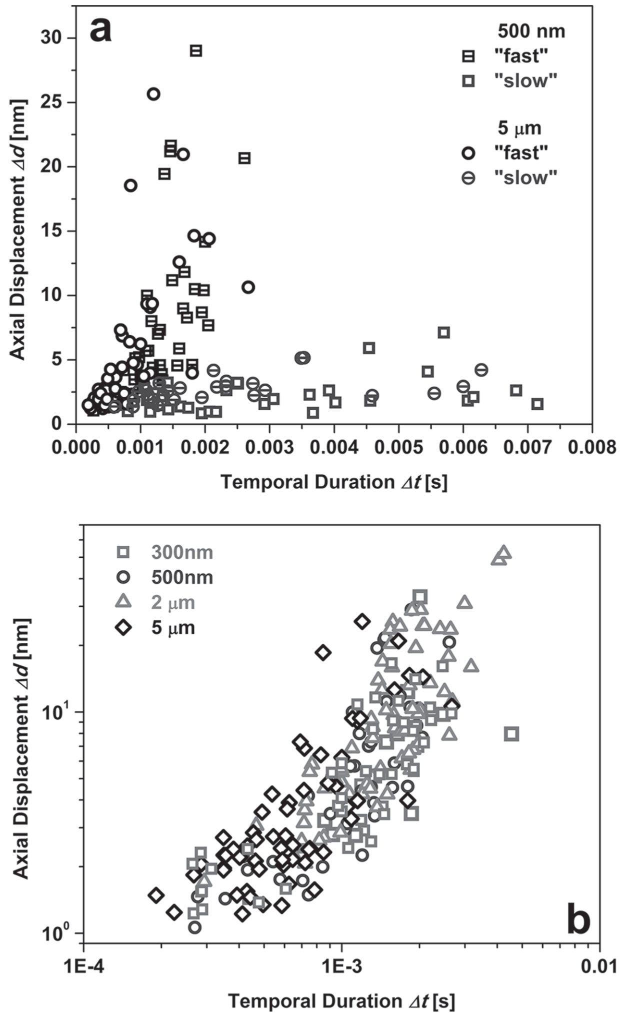

Figure 3. a) Δd vs. Δt for both types of events for a sample size of 500 nm and 5 mm. In (b) all "fast" events are summarized for all sample sizes.

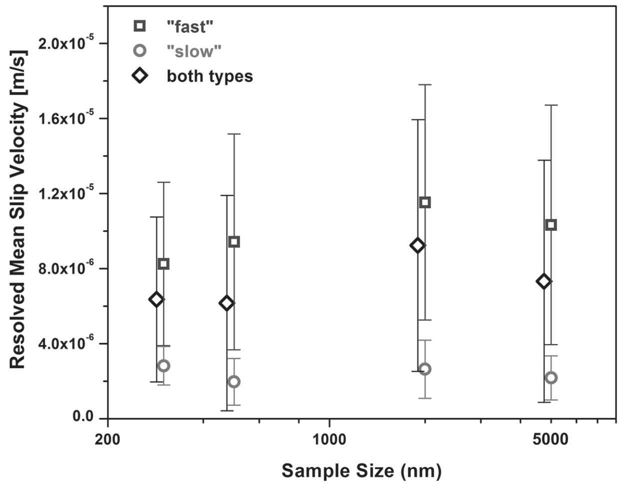

Figure 4. Resolved overall mean slip velocity for each sample size studied. Independent of sample size or event type, the velocity remains constant within the scatter of the data. The data points for both types of events have been shifted to the left by 5% to increase readability.

displacement jump with a rate higher than the temporal extension of the event. Figure 2d shows a displacement jump recorded with 60 Hz, representing an extreme case of under-sampling the slip event. We note that this DAR is still about 12 times higher than what was used in earlier work on Ni.[23,32] Here Δt will always be 1/60 s and thus yielding artificially slower slip (avalanche) velocities. For a precise determination of the dislocation avalanche's tempo-spatial extension, it is hence of importance to measure the transient events with a sufficiently high DAR, even though this can lead to a wealth of information that may not be completely analyzable, as shown in Figure 2c.

2.3. Slip Velocities as a Function of Sample Size, Applied Stress and Strain

As a first step both the axial displacements Δd as well as the corresponding temporal durations Δt are considered. **Figure 3**a summarizes these values for all of the investigated 500 nm and 5 μm specimens. From this figure it is clear that there are two regimes of data correlation, which separates the events into one group with low Δd but higher Δt values, and the other group contains higher axial displacement values in relation with smaller temporal durations. Comparing the raw data of both these different correlations, reveals that the above defined "fast" slip events follow the steep displacement-duration correlation, and that the "slower" slip events follow the lower correlation. At small times and displacements there is an overlap of both trends, which to a certain extent will be inseparable due to the nature of the recorded data. In addition to the two correlations in Figure 3a, the data for both 500 nm and 5 μm large crystals covers the same absolute regimes in both trends for both samples. This feature of the data can be visualized more clearly, when plotting all axial displacement values as a function of their temporal duration – now for all samples considered in this work. In Figure 3b only the regular "fast" events are considered, showing that the Δd and Δt values cover the same range independent of sample size. This result is also found for the "slow" events (not shown here).

Since the event sizes and temporal durations are similar for all studied sample sizes, it is instructive to plot the slip velocity as a function of sample size. For this, the axial displacement is resolved onto the {111}/⟨110⟩ slip system. **Figure 4**a displays the resolved overall mean slip velocity for both types of events as a function of sample size. The merged data for both types of events has been shifted to the left by 5% to improve readability of the graph. Overall the data displays a large amount of scatter, but more importantly for all event types ("fast" and "slow") a size-independent mean slip velocity $\overline{v}_{slip}$ is found. The mean velocity for the regular "fast" events is of the order of 10^{-5} ms^{-1}, while the "slow" events are on average 4–6 times slower.

While the mean slip velocity is independent of sample size, the influence of plastic strain and of applied stress is now investigated. **Figure 5**a summarizes the slip velocity as a function of plastic stain, and demonstrates a clear invariance of the resolved velocity with respect to engineering strain

DOI: 10.1002/smll.201400849

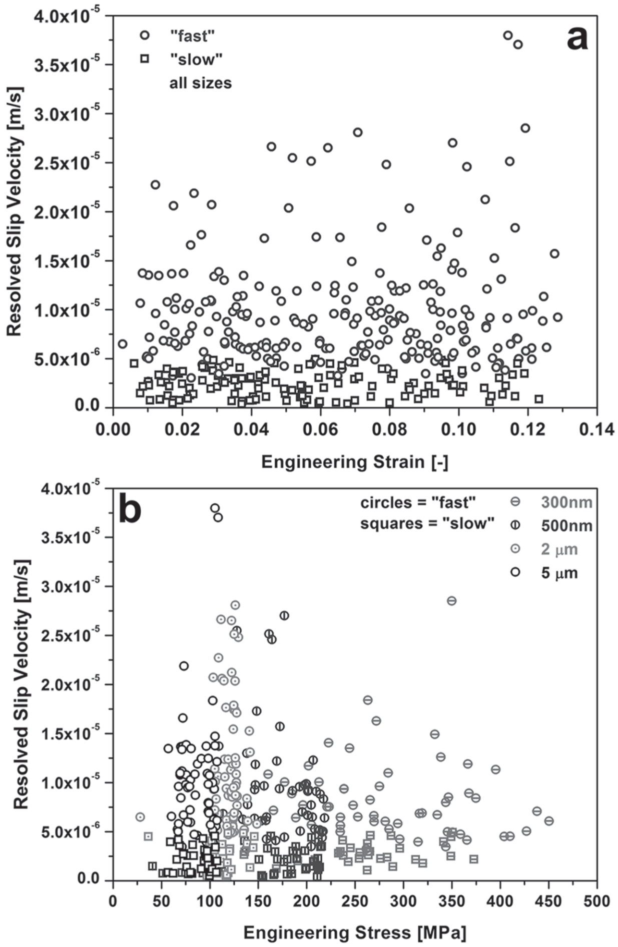

Figure 5. Resolved slip velocity as a function of engineering strain (a) and engineering stress (b) featuring no correlations with sample size.

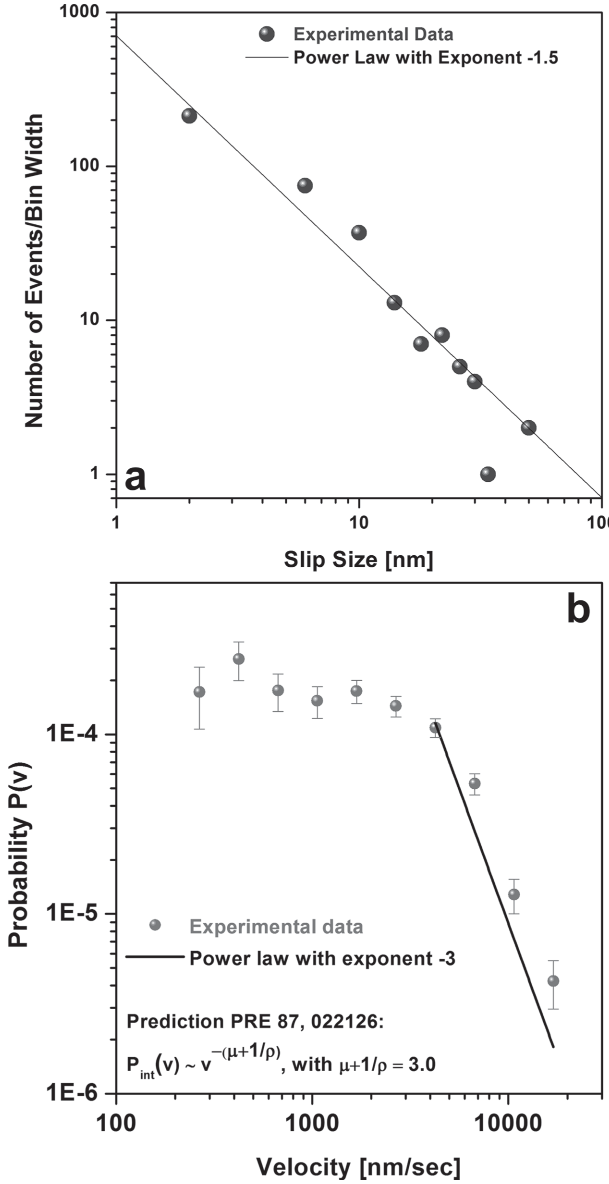

Figure 6. a) Stress-integrated frequency distribution of slip sizes for all slip events. The straight line indicates a power-law scaling with an exponent of 1.5; b) stress integrated velocity distribution that indicates a cubic decay at higher velocities and a plateau at the lower end.

for all specimen sizes. This invariance is equally present for both types of events. The data further shows a clear separation between the "faster" and "slower" events, which lies at around 3×10^{-6} ms^{-1}, consistent with the already depicted mean values in Figure 4. Remarkably, the same uncorrelated trend of slip velocity vs. applied engineering stress is found in Figure 5b. For a range between 50 MPa (5 μm specimen) and 450 MPa (300 nm specimen) the resolved mean slip velocity is independent of applied stress. The different stress ranges covered per sample size in Figure 5b are simply a result of the different apparent flow stress responses of the tested specimen. From Figure 5a and b it becomes evident that both types of events occur at all strains and stresses.

3. Discussion

3.1. Slip Size and Velocity Distribution

Theory and modeling predicts a power-law scaling of the stress-integrated slip-size distribution with a scaling exponent of ~1.5.[21,35] The same values are derived from the distribution of slip sizes of micro-compression experiments.[20,36] Thus, a good indication for the validity of the here obtained slip-sizes is to investigate the slip-size distribution of all crystal sizes. All slip-sizes are therefore binned and the resulting frequency distribution is displayed in **Figure 6**a. Despite the limited number of data points, the binned data shows a scaling that is in good agreement with a power-law with an exponent of ~1.5 for slip-sizes between ~1 nm to 60 nm, which is a typically reported value for stress-integrated slip size distributions.

Further evidence supporting that the slip velocities are directly reflecting the dynamics of the underlying dislocation dynamics can be made by plotting the stress integrated velocity distribution (Figure 6b). The experimental data in Figure 6b is compatible with a cubic decay at higher velocities, and therefore is in good agreement with predictions for slip velocities near the depinning transition, as indicated by the term of the mean-field critical exponents $(\mu+1/\sigma) = 3$,[37]

DOI: 10.1002/smll.201400849

as well as with the velocity distribution obtained via 3D dislocation dynamics simulations.[38] The same simulations also find the apparent shoulder at lower velocities, which have been associated with a quiescent avalanche state.

In addition to comparing the slip-size and slip-velocity distributions with theoretical predictions and other experimental data, it is of importance to verify if the used experimental set-up is capable of tracing the movement of the slipping crystal. Since the coupled mechanics of the device-sample assembly, including the PID-controlled feedback loop can only be modeled with a number of assumptions, we chose to directly test the contact between the compression tip and sample during the dynamic phase of the slip event. This is done by applying a constant voltage across the sample-tip connection, and recording the current with the same DAR applied to the force and displacement signal. It is found that, within the resolution of the experiment, no drop in current can be recorded throughout the displacement jump, clearly indicating that the mechanical sample-tip contact is maintained. Further details on these additional experiments are provided in the Supporting Information. The fact that our data aligns well with theoretical predictions, past dislocation dynamics modeling, as well as that the dynamics of the experiment are shown to remain coupled, suggests that we indeed are directly measuring the crystallographic slip phenomenon.

3.2. Assessment of the Derived Slip Velocities

A natural question that emerges is whether the measured slip or avalanche velocity can be linked to a dislocation velocity? For all types of events, the mean slip velocities are significantly smaller than dislocation (single and groups) velocities reported for pure fcc metals in earlier work,[3,4] where speeds of ~10^{-1} to 10^{1} ms^{-1} have been reported. A direct correlation between the dislocation velocity and the here determined slip (dislocation avalanche) velocities is not straight forward. Becker and Haasen showed that the growth rate of a slip step height (equivalent to the resolved value of $\Delta d/\Delta t$) is proportional to the dislocation velocity v:[39]

$$\frac{\Delta d}{\Delta t} = v \times b \times \sin(\delta) \times \frac{1}{x_{dis}}, \tag{1}$$

where δ is the angle between the surface normal and the slip plane, and x_{dis} the average dislocation distance: a quantity that is not accessible to direct measurements. This model was extensively used in slip line cinematography for investigations of slip step growth normal to the surface.[11–13,40] In the same studies, the velocity of groups of dislocations was determined along the slip line growth direction, where the velocity can be directly derived from the propagating front and x_{dis} is not required. In previous work[41] we derived a proportionally between the measured axial displacement velocity v_{ad} and a dislocation avalanche velocity $v_{Avalanche}$

$$v_{ad} \propto \rho \Delta d l b \times v_{Avalanche}, \tag{2}$$

with b the Burgers vector, l characteristic length of a mobile dislocation segment, d the sample diameter, and ρ the volumetric dislocation density. Equations (1) and (2) both suggest that $\bar{v}_{Avalanche} \propto \bar{v}_{Dislocations}$ – a result that will be assumed in the remainder of this work. In making this connection between slip/avalanche velocity and dislocation velocity, it then becomes remarkable that the experimentally derived data of section 2 does not show any notable trends. This is particularly surprising, because one might expect that $\bar{v}_{Avalanche} = f(\tau_{appl})$. Indeed, the stress insensitivity of the data implies that the underlying micro structural length scales (ρ, l, and x_{dis}) are not changing across the conducted experiments, or that the scatter, caused by the local micro structural environment for each dislocation avalanche contained in Figure 4 and Figure 5 obscures any effects as entailed by both equations (1) and (2), or similar derivations. In the next section these aspects will be discussed.

3.3. Independence of Slip Velocities on Plastic Strain and Applied Stress

3.3.1. Experimental Observations

Most generally the velocity of individual dislocations and also groups of dislocations has been shown to strongly depend on applied stress τ_{appl}. In the low velocity regime ($\bar{v}$ < ~10 ms^{-1}) thermal activation controls the velocity, which can be described by either a power-law:

$$\bar{v} = v_0(\tau_{appl} / \tau_0)^n, \tag{3}$$

with v_0 being a reference velocity of 1 cms^{-1} defined at a reference stress τ_0 and with $n(>>1)$; or by the Arrhenius-type relationship:

$$\bar{v} = v_1 \times \exp\left[-(\Delta G_0 - V(\tau_{appl})\tau_{appl}) / kT\right], \tag{4}$$

where v_1 is a unit velocity, ΔG_0 an activation energy, $V(\tau_{appl})$ the activation volume, k the Boltzmann factor and T the temperature.[18] The controlling mechanisms behind thermally activated dislocation motion have been explored intensely,[14,18] and can be summarized as being either localized or linear barriers such as forest dislocations, solute atoms and clusters, precipitates, cross slip, or the Peierls-Nabarro stress. However, in the present work the resolved slip velocity, does not exhibit any notable dependence on applied stress (Figure 5b), and therefore does not follow Equation (3) or (4). How can this be explained? Firstly, it is clear that the dislocations participating in an avalanche require a driving force in order to be initiated, which, if not correlated with the externally applied stress, must then originate from the influence of internal stress field fluctuations that are known to be present in any kind of realistically dislocated crystal.[42,43] Two interpretations are proposed, of which the first one is based on the existence of a static random internal stress field (**Figure 7**). The second interpretation takes into account dynamical changes of internal stresses occurring during the dislocation avalanche, and will be more closely discussed after the dislocation dynamics simulation results in section 3.3.2.

small 2014,
DOI: 10.1002/smll.201400849

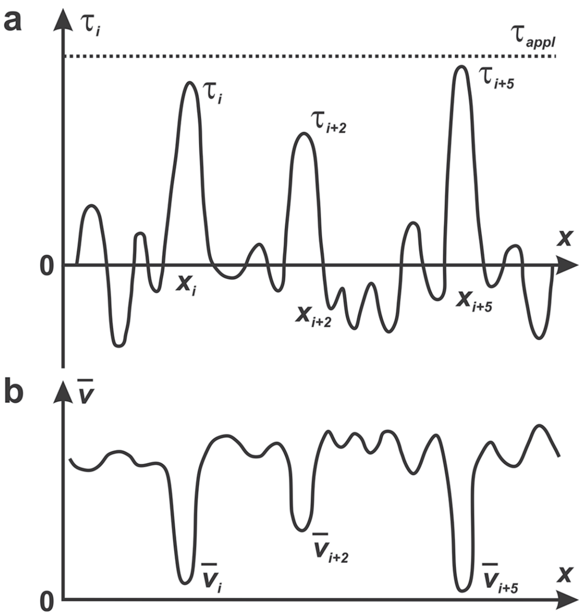

Figure 7. a) A randomly fluctuating internal stress field along a given direction x in the crystal. At positions x_i, x_{i+2} and x_{i+5} the internal stress τ_i rises to values close to the externally applied stress τ_{appl}. As a result, dislocations propagating through this static stress field will spend most of their time residing in the regions close to x_i, x_{i+2} and x_{i+5} where the velocities are the lowest (b). These low velocities dominate the mean velocity derived for the total distance along x.

Figure 7a schematically displays a randomly varying internal stress τ_i along any coordinate axis x within the crystal lattice. The presence of internal stress fields influencing the velocity of dislocations has been investigated theoretically with strongly varying conclusions.[44–46] Common to these approaches is the consideration of the applied stress τ_{appl} being the sum of an internal stress and an effective stress τ_e:

$$\tau_{appl} = \tau_i(x) + \tau_e, \tag{5}$$

Locally, the difference between the externally applied stress τ_{appl} and the internal stress $\tau_i(x)$ must be proportional to the driving force of the dislocation. Under conditions when τ_{appl} just slightly exceeds the peak internal stresses, the moving dislocation(s) will be very slow because of the low difference of τ_{appl}-$\tau_i(x)$ (Figure 7b). The experimentally determined dislocation velocity in such a scenario is dominated by the time t_i spent at positions x_i with almost equal applied stress and internal stress. Nabarro and Conrad proposed this picture for low speed dislocation velocities, in which case the mean dislocation velocity over a distance x will be given by:[46]

$$\bar{v} = \frac{x}{\int_0^x \frac{dx}{v}} \approx \frac{x}{\sum_i \Delta t_i} \tag{6}$$

with v being a local velocity, and Δt_i the time the dislocation spends at each position x_i of high internal stresses. For the present work, this interpretation necessarily implies that the difference between the applied stress and the internal stress must be on average the same, independent of *both* strain and sample size. An on average constant τ_{appl}-$\tau_i(x)$ as a function of strain can be understood as follows: various experimental reports have shown that the dislocation density does not notably change as a function of strain during extended plastic flow,[47,48] which also is compatible with theoretical models that explain the strong size-dependence in stress at this scale.[31,49–51] It is important to keep in mind that this constant dislocation density only applies for the regime beyond the apparent yield stress; that is beyond the break-away stress. While the dislocation density can be taken as invariant during extended plastic flow, it can increase before the extended flow regime is reached.[47,48,52] This increase has been reported to be more pronounced in smaller samples covering 1 to 10 μm in diameter.[48] Therefore, the interpretation based on a static internal stress field governing the measured average dislocation velocity may hold for a constant sample size, but does not explain how an on-average constant τ_{appl}-$\tau_i(x)$ as a function of crystal size can emerge. In addition, there are numerous other defects introduced during sample preparation that will affect the internal stress landscape; a topic that has been discussed intensely with respect to size-affected plasticity of dislocated single crystals.[49,53–56] In order to include the dynamics of the evolving internal stresses during rearrangements of the dislocation network, τ_{appl}-$\tau_i(x,t)$, dislocation dynamics simulations have been conducted that will be outlined in the following section.

3.3.2. Dislocation Dynamics Simulations

To better understand the fundamental origin of the invariant dislocation avalanche velocity, a simplified dislocation dynamics model is used in which a dipolar dislocation mat is embedded into an internal static sinusoidal stress field defined by a wave-length (λ) and a shear-stress amplitude (τ_0). Here the explicit dislocation population of the dipolar mat represents the mobile dislocation content and the internal shear-stress field represents a mean-field description of the immobile dislocation content. Despite its simplicity, the model exhibits intermittent plasticity and a corresponding scale-free avalanche phenomenon for the distribution of strain burst magnitudes, obtaining an exponent similar to those seen in experiment and more complex dislocation dynamics simulations. More details of this model may be found in the literature.[57]

The dipolar mat contains equal numbers of dislocations of opposite Burgers vector embedded in a static sinusoidal internal stress field, defined by

$$\tau_i(x) = \tau_0 \cos\left(\frac{2\pi x}{\lambda}\right), \tag{7}$$

where the direction x is along the dipolar mat direction. Periodic boundary conditions are assumed along x with a commensurate (to λ) periodic length, d. The equation of motion along the x direction for the ith dislocation is given by

$$\frac{\delta x_i}{\delta t} = \frac{1}{B}\left[\tau_{appl} - \tau_i(x_i) - \sum_{j\neq i}\tau_{ij}\right] b_{x,i}, \tag{8}$$

DOI: 10.1002/smll.201400849

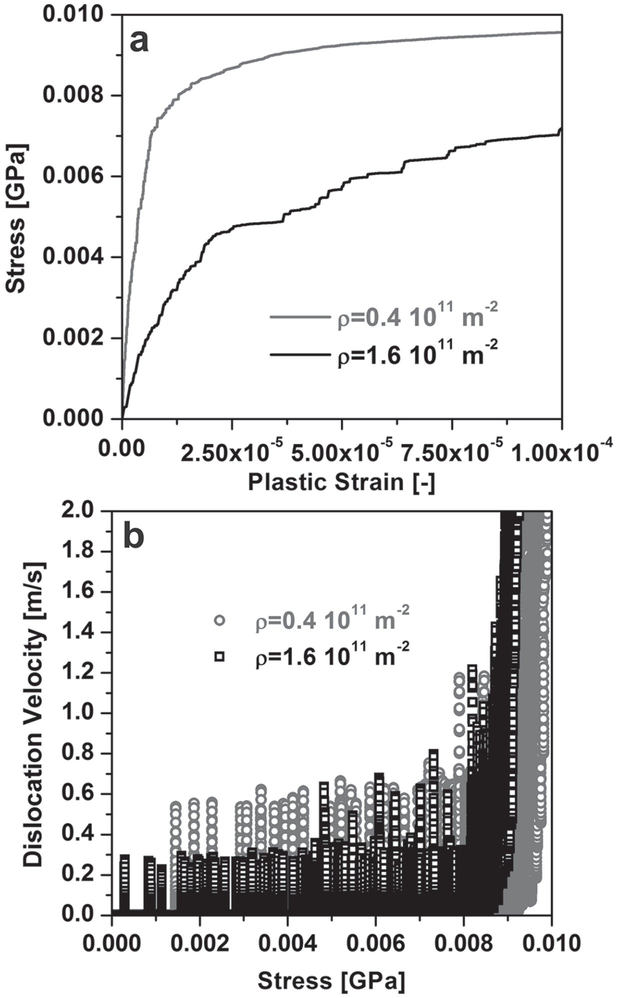

Figure 8. a) Stress versus plastic strain curves for two mobile dislocation densities; b) mean dislocation velocity as a function of external stress.

where B is the damping coefficient and τ_{ij} is the shear stress felt by dislocation i due to dislocation j. In Ref. [57], an exact expression for τ_{ij} in the dipolar mat geometry is given that takes into account all periodic image effects of two parallel slip planes. τ_{appl} is again the external homogeneous applied stress field. Equation (8) is a first order differential equation and thus all dynamics are assumed to be in the over damped regime.

Figure 8a shows the stress versus plastic strain curves for the parameter set $\lambda = 2$ microns, $d = 400$ microns and $\tau_0 = 10$ MPa. The simulations are performed under a constant stress-rate loading mode. For the material parameters, a model Cu system is assumed since there exists a well accepted value for the damping coefficient. Although, quantitatively specific to Cu, the simulation results are expected to be similar for all simple FCC systems including that of Au. Two *mobile* dislocation density values are simulated with $\rho = 0.4 \times 10^{11}$ m^{-2} and $\rho = 1.6 \times 10^{11}$m^{-2}. In Figure 8a, the small values of plastic strain demonstrate that the curves are predominantly in the micro-plastic regime. Both curves exhibit intermittent plasticity, which in terms of plastic strain burst magnitude distribution has been shown to be scale-free.[57] Figure 8b now shows the mean dislocation velocity within the system, indicating a singular structure that correlates with the occurrence of discrete plastic strain events seen in Figure 8a. Both data sets show that at high enough applied stress (and plastic strain), the mean velocity begins to rapidly increase corresponding to the onset of macroscopic plasticity and therefore yield. Indeed, the approximately linear relation between velocity and applied stress in this flow regime is precisely that of the employed linear microscopic mobility law used in the simulations. More relevant to the current work is the observation that within the micro-plastic regime, typical dislocation velocities are insensitive to the applied stress value at which they occur – a result entirely consistent with the experimental results of section 2.

Figures 9a to c (upper panel) plot, for selected dislocations that have participated in an irreversible structural transformation within the micro-plastic regime, the three stress contributions of Equation (8). These stresses are plotted as a function of applied shear stress. Also shown (Figures 9d–f, lower panels) is the corresponding mean dislocation velocity for all mobile dislocations. Figure 9 is taken from the loading simulation with the mobile dislocation density equal to $\rho = 1.6 \times 10^{11}$m^{-2}. Inspection of Figure 9 reveals that the rapid local variation in stress that these dislocations experience is due to both the internal static stress field, and also a purely dynamical component arising from the other dislocations. The latter contribution is found to increase with increasing dislocation density (not shown here). Importantly, as a function of applied stress, the rapid variation in the internal stress component remains approximately constant at a stress of ~ $0.5 \times \tau_0$.

The picture that therefore emerges from the present simulations is that the motion of a dislocation during an irreversible structural transformation within the micro-plastic regime is primarily controlled by the internal stress field that is, in part, static (due to the static sinusoidal field) and, in part, dynamic (due to the other dislocations). The externally applied stress field therefore plays a relatively minor role in determining the dislocation velocities during the evolution of the plastic event when in the micro-plastic regime. The fluctuations in the mean mobile dislocation velocities are thus mainly due to fluctuations in the number of dislocations participating in any one discrete plastic event, but also due to the increasing dynamical fluctuations in internal stress with increasing dislocation content. Despite the disparity in the velocity scale between athermal dislocation dynamics simulations and thermal activation which dominates the experimental findings, these dislocation dynamics simulations suggest that the dynamics of the internal stress fields during a dislocation avalanche are responsible for the same stress-independent mean dislocation avalanche velocity observed experimentally at all sample sizes. In fact, this suggests that the internal stress field structure and thus the microstructure remains on average unaltered during plastic flow at all sizes studied.

3.4. Separating Micro-Plastic and Macro-Plastic Flow

Both experiments and simulations reveal a regime of dislocation (avalanche) velocities that is independent of applied

small 2014,
DOI: 10.1002/smll.201400849

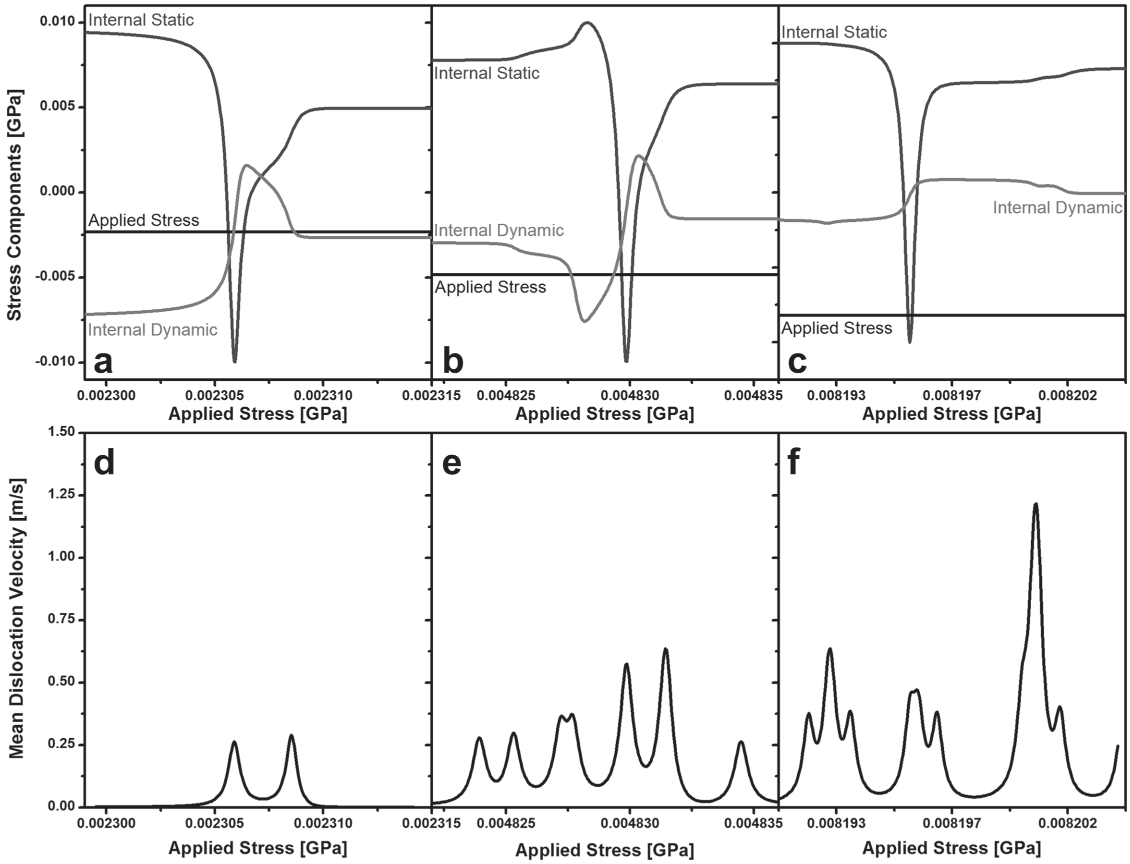

Figure 9. a–c) Individual stress components on selected dislocations (internal static stress is equal to $\tau_i(x)$, external applied stress is equal to $-\tau_{appl}$, and the internal dynamical stress is given by the stress due to all other mobile dislocations within the system). d–f) Corresponding mean dislocation velocity to (a–c). Data is taken for a mobile dislocation density equal to $\rho = 1.6 \times 10^{11}\,m^{-2}$, and all three examples were taken in the micro-plastic regime of deformation (see Figure 8).

stress. The dislocation dynamics simulations on bulk crystals show, that this regime corresponds to strains prior to the macroscopic yield stress. This regime is macroscopically elastic, but is also known to include numerous local plastic transitions, which typically is referred to as the micro-plastic regime. First at the macroscopic yield transition and beyond, the simulations show the expected velocity-stress scaling. Similarly, the classic experiments which found a velocity-stress scaling as captured by Equation (3) or (4) were mostly performed at stresses past or above the yield stress. On the basis of this, we conclude that micro-plastic and macro-plastic flow can be distinguished by the inherent stress-velocity scaling of the dislocations, which we summarize schematically in **Figure 10**.

It is noted that the transition regime between the stress-independent micro-plastic regime and the strong stress-velocity scaling during macro-plastic flow is not captured by the experiments, but only by the simulations. It's precise nature is not yet fully investigated, but believed to originate from the de-pinning transition for a dislocation that is used to define the transition to extended plastic flow.[35] Indeed the schematic is not so dissimilar to the generic velocity versus applied stress curve demonstrating the depinning transition (see for example Figure 3 of ref. [35]). Figure 10 further entails that samples belonging to the size-regime studied here (300 nm to 5 μm) deform equivalently to bulk crystals during micro-plastic flow. As mentioned earlier, it has been reported that there is very little change of the dislocation structure throughout extended flow of the types of samples tested here, which is compatible with the micro-plasticity

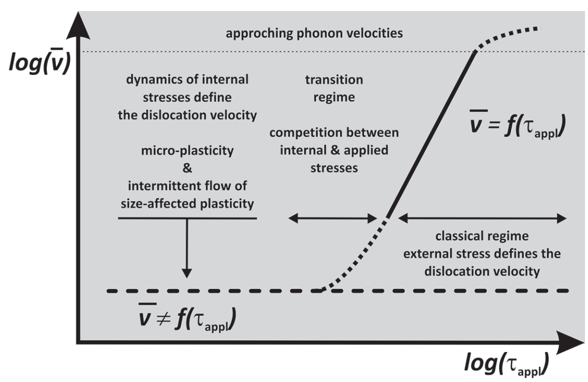

Figure 10. A schematic summary of the dislocation velocity scaling with respect to applied stress. At low stresses below the yield stress – the micro-plastic regime – the dislocation velocity is independent of the applied stress. In this regime the dynamics of internal stress fields governs the dislocation velocity, and is the regime that dominates the plasticity of small scale crystals. With increasing stress the regime of the classical velocity-stress scaling is reached in which the externally applied stress governs the dislocation velocity.

of bulk crystals; a regime in which no significant changes in microstructure occur during straining.[58]

4. Conclusion

This work investigates the spatiotemporal signature of displacement bursts measured during micro-compression of cylindrical Au single crystals covering a diameter range between 300 nm and 5 µm. A large scatter of slip velocities is observed, which neither exhibits a resolvable trend with applied stress with a range of 40 to 450 MPa, nor with plastic strain. The stress integrated slip-size and slip-velocity distributions reveal power-law scaling regimes as expected for crystal plasticity, indicating that the obtained slip velocity is representative of a dislocation phenomenon. Assuming that displacement bursts correspond to a dislocation avalanche, a mean dislocation avalanche velocity is derived from the spatio-temporal extent of these bursts. To better rationalize the stress-insensitivity of the spatiotemporal slip event, complementary dislocation dynamics simulations on a model bulk crystal is performed. These simulations show that at small plastic strains in the micro-plastic regime of the bulk crystal the underlying dislocation velocities are insensitive to the applied stress. This leads to the final proposition that plasticity in nano- or micro-pillars is dynamically equivalent to the micro-plasticity of macroscopic systems, and that the scaling between applied stress and dislocation velocity can be used to discriminate between these two very distinct regimes of plasticity.

5. Experimental Section

Cylindrical pillars were prepared with focused ion-beam (FIB) milling from a gold single crystal that was grown from the melt. A sequential milling procedure was used, where the outer diameter was reduced stepwise. With each milling step the ion current was lowered to minimize structural damage of the crystals, finally using a surface polishing step with 30 pA. Care was taken to minimize sample tapering, which was measured to be on average ~1.16°. Even though this value is small, geometrical hardening as a result of a stress gradient cannot be excluded. The samples had an aspect ratio between 2.6 and 3 for sizes between 500 nm and 5 µm, and up to 4 at the smallest diameter. All samples had a [001] high-symmetry compression-axis, which allows the activation of all twelve slip systems upon deformation and which minimizes crystal rotation during deformation.

Micro-compression testing was performed with a Hysitron Triboscope nanoindenter controlled by a Performec hardware. This steering module runs with a feedback control loop frequency of 78 kHz, and allows to record ~200 000 data points per test. Thus, dependent on the total test time, the data acquisition rate (DAR) can be chosen to a maximum value. A conical diamond tip with a flat end of either 9 or 15 µm was used for compression at a nominally applied strain rate of 5×10^{-3} s^{-1} in displacement controlled mode. In order to verify that the sample-plate contact was maintained during the slip event, in-situ electrical measurements were conducted. In these additional tests, a constant voltage was applied over the sample, and the current was monitored with the same DAR as the mechanical data.

Supporting Information

Supporting Information is available from the Wiley Online Library or from the author.

Acknowledgements

R.M. also thanks the Alexander von Humboldt foundation for financial support during his stay at Caltech, and his host G.M. Pharr for valuable discussions. J.R.G. and R.M. would also like to thank the Office of Naval research, grant Nr. ONR Grant N000140910883.

[1] W. G. Johnston, J. J. Gilman, *J. Appl. Phys.* **1959**, *30*, 129–144.
[2] D. F. Stein, J. R. Low, *J. Appl. Phys.* **1960**, *31*, 362–369.
[3] H. Suga, T. Imura, *Trans. Jpn. Inst. Met.* **1976**, *17*, 605–614.
[4] P. Vr, J. Weertman, N. Urabe, *J. Appl. Phys.* **1972**, *43*, 2982–&.
[5] E. B. Leiko, D. V. Lotsko, E. M. Nadgornyi, V. I. Trefilov, *Fiz. Tverd. Tela* **1975**, *17*, 2735–2742.
[6] N. Urabe, J. Weertman, *Mater. Sci. Eng.* **1975**, *18*, 41–49.
[7] H. Traub, H. Neuhauser, C. Schwink, *Acta Metall.* **1977**, *25*, 437–446.
[8] D. P. Pope, T. Vreeland, *Philos. Mag.* **1969**, *20*, 1163–&.
[9] E. Y. Gutmanas, E. M. Nadgornyi, A. V. Stepanov, *Soviet Physics-Solid State* **1963**, *5*, 743–747.
[10] H. D. Guberman, *Acta Metall.* **1968**, *16*, 713–721.
[11] M. Kugler, A. Hampel, H. Neuhauser, *Phys. Status Solidi A* **1999**, *175*, 513–526.
[12] A. Hampel, H. Neuhauser, *Phys. Status Solidi A* **1987**, *104*, 171–181.
[13] O. B. Arkan, H. Neuhauser, *Phys. Status Solidi A* **1987**, *99*, 385–397.
[14] E. Nadgornyi, *Prog. Mater. Sci.* **1988**, *31*, 1–530.
[15] K. M. Jassby, T. Vreeland, *Philos. Mag.* **1970**, *21*, 1147–&.
[16] M. Kleintges, P. Haasen, *Scr. Metall.* **1980**, *14*, 999–1003.
[17] H. Saka, T. Imura, *Phys. Status Solidi A* **1973**, *19*, 653–660.
[18] H. Neuhäuser, in *Dislocations in Solids*, *Vol. 6* (Ed: F. R. N. Nabarro), North-Holland Publishing Company, Amsterdam, **1983**, pp. 319–440.
[19] M. Zaiser, J. Schwerdtfeger, A. S. Schneider, C. P. Frick, B. G. Clark, P. A. Gruber, E. Arzt, *Philos. Mag.* **2008**, *88*, 3861–3874.
[20] D. M. Dimiduk, C. Woodward, R. LeSar, M. D. Uchic, *Science* **2006**, *312*, 1188–1190.
[21] F. F. Csikor, C. Motz, D. Weygand, M. Zaiser, S. Zapperi, *Science* **2007**, *318*, 251–254.
[22] M. D. Uchic, D. M. Dimiduk, J. F. Florando, W. D. Nix, *Mat. Res. Soc. Symp. Proc.* **2003**, *753*, 27–34.
[23] M. D. Uchic, D. A. Dimiduk, *Mater. Sci. Eng. A* **2005**, *400*, 268–278.
[24] M. B. Lowry, D. Kiener, M. M. LeBlanc, C. Chisholm, J. N. Florando, J. W. MorrisJr, A. M. Minor, *Acta Mater.* **2010**, *58*, 5160–5167.
[25] F. Mompiou, M. Legros, A. Sedlmayr, D. S. Gianola, D. Caillard, O. Kraft, *Acta Mater.* **2012**, *60*, 977–983.
[26] S. Korte, M. Ritter, C. Jiao, P. A. Midgley, W. J. Clegg, *Acta Mater.* **2011**, *59*, 7241–7254.
[27] R. Maass, S. Van Petegem, H. Van Swygenhoven, P. M. Derlet, C. A. Volkert, D. Grolimund, *Phys. Rev. Lett.* **2007**, *99*, 145505.

DOI: 10.1002/smll.201400849

[28] R. Maass, S. Van Petegem, D. Grolimund, H. Van Swygenhoven, D. Kiener, G. Dehm, *Appl. Phys. Lett.* **2008**, *92*, 071905.
[29] C. Kirchlechner, D. Kiener, C. Motz, S. Labat, N. Vaxelaire, O. Perroud, J. S. Micha, O. Ulrich, O. Thomas, G. Dehm, J. Keckes, *Philos. Mag.* **2011**, *91*, 1256–1264.
[30] M. D. Uchic, D. M. Dimiduk, J. N. Florando, W. D. Nix, *Science* **2004**, *305*, 986–989.
[31] J. R. Greer, W. C. Oliver, W. D. Nix, *Acta Mater.* **2005**, *53*, 1821–1830.
[32] C. P. Frick, B. G. Clark, S. Orso, A. S. Schneider, E. Arzt, *Mater. Sci. Eng. A* **2008**, *489*, 319–329.
[33] C. A. Volkert, E. T. Lilleodden, *Philos. Mag.* **2006**, *86*, 5567–5579.
[34] R. Maass, S. Van Petegem, D. Ma, J. Zimmermann, D. Grolimund, F. Roters, H. Van Swygenhoven, D. Raabe, *Acta Mater.* **2009**, *57*, 5996–6005.
[35] M. Zaiser, *Adv. Phys.* **2006**, *55*, 185–245.
[36] N. Friedman, A. T. Jennings, G. Tsekenis, J.-Y. Kim, M. Tao, J. T. Uhl, J. R. Greer, K. A. Dahmen, *Phys. Rev. Lett.* **2012**, *109*, 095507.
[37] M. LeBlanc, L. Angheluta, K. Dahmen, N. Goldenfeld, *Phys. Rev. E* **2013**, *87*, 13.
[38] P. D. Ispanovity, I. Groma, G. Gyorgyi, F. F. Csikor, D. Weygand, *Phys.Rev.Lett.* **2010**, *105*, 085503.
[39] R. Becker, P. Haasen, *Acta Metall.* **1953**, *1*, 325–335.
[40] H. H. Potthoff, *Phys. Status Solidi A* **1983**, *77*, 215–224.
[41] R. Maass, P. M. Derlet, J. R. Greer, *Scr. Mater.* **2013**, *69*, 586–589.
[42] I. Gaal, T. Geszti, *Scr. Metall.* **1969**, *3*, 133–138.
[43] U. F. Kocks, *Acta Metall.* **1967**, *15*, 1415–1417.
[44] W. D. Nix, W. A. Coghlan, C. R. Barrett, *Mater. Sci. Eng.* **1969**, *4*, 98–&.
[45] F. Guiu, *Phys. Status Solidi A* **1969**, *33*, 785–&.
[46] F. R. N. Nabarro, H. Conrad, *Low-Speed Dislocations*, New York **1968**.
[47] S. H. Oh, M. Legros, D. Kiener, G. Dehm, *Nat.Mater.* **2009**, *8*, 95–100.
[48] D. M. Norfleet, D. M. Dimiduk, S. J. Polasik, M. D. Uchic, M. J. Mills, *Acta Mater.* **2008**, *56*, 2988–3001.
[49] J. R. Greer, W. D. Nix, *Phys. Rev. B* **2006**, *73*, 245410.
[50] S. I. Rao, D. M. Dimiduk, T. A. Parthasarathy, M. D. Uchic, M. Tang, C. Woodward, *Acta Mater.* **2008**, *56*, 3245–3259.
[51] P. M. Derlet, R. Maass,Philos. Mag., 2014, DOI:10.1080/14786435.2014.932502.
[52] R. Maass, M. D. Uchic, *Acta Mater.* **2012**, *60*, 1027–1037.
[53] D. Kiener, C. Motz, M. Rester, M. Jenko, G. Dehm, *Mater. Sci. Eng. A* **2007**, *459*, 262–272.
[54] R. Maass, S. Van Petegem, J. Zimmermann, C. N. Borca, H. Van Swygenhoven, *Scr. Mater.* **2008**, *59*, 471–474.
[55] R. Maass, D. Grolimund, S. Van Petegem, M. Willimann, M. Jensen, H. Van Swygenhoven, T. Lehnert, M. A. M. Gijs, C. A. Volkert, E. T. Lilleodden, R. Schwaiger, *Appl. Phys. Lett.* **2006**, *89*, 151905.
[56] A. T. Jennings, M. J. Burek, J. R. Greer, *Phys. Rev. Lett.* **2010**, *104*, 135503.
[57] P. M. Derlet, R. Maass, *Modell. Simul. Mater. Sci. Eng.* **2013**, *21*, 035007.
[58] C. J. McMahon, *Microplasticity*, Interscience, New York **1968**.

Received: March 28, 2014
Published online: